Journal of Fluorescence, Vol. 15, No. 5, September 2005 (© 2005)
DOI: 10.1007/s10895-005-2978-4

Improved Fluorescent Proteins for Single-Molecule Research in Molecular Tracking and Co-Localization

Ralf Steinmeyer,[1,3] Andrey Noskov,[1,3] Cornelius Krasel,[2,3] Isabell Weber,[1] Christian Dees,[2] and Gregory S. Harms[1,4]

Received March 22, 2005; accepted July 22, 2005

Three promising variants of autofluorescent proteins have been analyzed photophysically for their proposed use in single-molecule microscopy studies in living cells to compare their superiority to other fluorescent proteins previously reported regarding the number of photons emitted. The first variant under investigation the F46L mutant of eYFP has a 10% greater photon emission rate and >50% slower photobleaching rate on average than the standard eYFP fluorophore. The monomeric red fluorescent protein (mRFP) has a fivefold lower photon emission rate, likely due to the monomeric content, and also a tenfold faster photobleaching rate than the DsRed fluorescent protein. In contrast, the previously reported eqfp611 has a 50% lower emission rate yet photobleaches more than a factor 2 slowly. We conclude that the F46L YFP and the eqfp611 are superior new options for single molecule imaging and tracking studies in living cells. Studies were also performed on the effects of forced quenching of multiple fluorescent proteins in sub-micrometer regions that would show the effects of dimerization at low concentration levels of fluorescent proteins and also indicate corrections to stoichiometry patterns with fluorescent proteins previously in print. We also introduce properties at the single molecule level of new FRET pairs with combinations of fluorescent proteins and artificial fluorophores.

KEY WORDS: Single-molecule microscopy; green fluorescent protein; fluorescence energy transfer (FRET); membrane biophysics; photophysics.

INTRODUCTION

In the past two decades, an exponential leap in knowledge has occurred by the use of fusion proteins of fluorescent proteins from various Hydrozoa and Anthozoa, most notably the green fluorescent protein (GFP) from the jellyfish *Aequorea victoria*. These proteins have been used to determine cellular localization, protein stability, protein colocalization and conformational changes in proteins. The development of different GFP variants by random mutagenesis has overcome obstacles such as slow maturation rates, dimerization or oligomerization, sensitivity to environmental ions, or photobleaching. Two new variants which exemplify these improved fluorescent proteins are the F46L mutation of enhanced yellow fluorescent protein (EYFP) [1] (F46L YFP) and the monomeric red fluorescent protein mRFP1 [2].

F46L YFP shows a faster maturation rate caused by accelerated oxidation of the chromophore. As a result, the fluorescence has been reported to be 20-fold stronger than that of standard EYFP [3]. It is therefore considered a superior acceptor fluorophore when performing fluorescence resonance energy transfer (FRET) experiments because it is preferred if the acceptor fluorophore matures quicker than the donor fluorescent protein, which is usually cyan fluorescent protein (CFP). F46L YFP shows also decreased sensitivity to pH and chloride concentrations

[1] Rudolf-Virchow-Center, DFG Research Center for Experimental Biomedicine, University of Würzburg, Versbacher Street, Würzburg, Germany.
[2] Institute of Pharmacology, University of Würzburg, Versbacher Street, Würzburg, Germany.
[3] Authors contributed equally to this article.
[4] To whom correspondence should be addressed. E-mail: gregory.harms@virchow.uni-wuerzburg.de

in the environment as compared to EYFP. However, the absorption and emission maxima, as well as the fluorescence quantum yield remained unchanged as compared to EYFP, while the absorption coefficient drops slightly from 80,000 to 78,000 M^{-1} cm^{-1}. Thus, it is not clear why or how the fluorophore could be brighter when from the definition of brightness, $B = \varepsilon \cdot \Phi_F$ (B = brightness, ε = absorptions coefficient, and Φ_F = fluorescence quantum yield), these fluorophores are equal. Some reasons could be that this definition does not include any parameters for stability, e.g., resistance to photobleaching, dark state kinetics due to protein conformational changes, protonation states, sensitivity to other ions and changes in fluorescence life time.

mRFP1 is a mutant of DsRed which reduces its propensity to aggregate. DsRed behaves as an obligate tetramer which limits its usefulness for fusion proteins since aggregation may impart the functionality of the fusion partner. The inclusion of 33 mutations resulted in a protein which behaved as a monomer, even at high concentrations [4]. Another advantage of mRFP1 over DsRed is its fast maturation time. Unfortunately, the fluorescence of mRFP1 is reduced to approimately 25% of that of DsRed, owing to a reduction in both the fluorescence quantum yield and the extinction coefficient.

Single-molecule microscopy was originally performed with small-molecule fluorophores which were introduced either by covalent linkage or antibodies. However, in living cells these methods allow access to cell surface proteins only. Therefore, it is of interest to develop other techniques to investigate intracellular proteins, for example by employing fusion proteins with fluorescent proteins. It was shown previously that EYFP and particularly DsRed offer particular advantages for visualizing single molecules in living cells, owing to their red-shifted emission spectrum [5]. This sets them apart from the intracellular background fluorescence which is mostly caused by flavins [6].

The eq611fp is an interesting variant developed and previously reported to be excellent for single-molecule studies [7–9]. It has the unique property of having a further red shift or stokes shift in the emission maximum and also matures very quickly, both with respect to the more ubiquitous DsRed. This fluorescent protein variant originates from the sea anemone *Entacmaea quadricolor*. The methods used to test this were confocal techniques of imaging, fluorescence correlation spectroscopy, time correlated single-photon counting, and spectral analysis. Since the protein seems to be monomeric, bright, and photostable in comparison to DsRed and to the other variants, it seemed a logical choice to test it for single-molecule tracking analysis.

This initial part of this study was performed to test the suitability of F46L YFP and mRFP1 for single-molecule applications. We have characterized these two fluorescent proteins by methods previously developed by us and others [10]. In particular, we were interested to elucidate the photophysical reasons for the apparent improvement in the brightness of EYFP F46L in the absence of a change in absorption coefficient and fluorescence quantum yield. With respect to mRFP1 we were interested if this monomeric protein can be detected at the single-molecule level.

Single-molecule tracking with the fluorescent proteins has only been applied in a low number of cases [11–13]. This is primarily due to the higher excitation intensities required to acquire photons for a brief integration period before the next exposure occurs. Because of the high excitation intensity which leads to fast photobleaching, individual single-molecule tracking appears to be limited to a very low number of tracking steps which were originally reported to be on average three steps for the eYFP variant.

Thus, with limited tracking ability for any single-molecule technique, it is better to center one's attention on single-molecule co-localization studies because one can get an approximate sense of the localization of one or more particles from a single diffraction limited fluorescence spot. This investigation involves to localize and quantify the number of fluorophores type per scanning region, typically down to the diffraction limit although with various techniques, superior resolution is possible [14,15]. This method of the determination of the local stoichiometry by single-molecule analysis was first reported by Schmidt *et al.* [16] for artificial systems and first applied to living cells by Harms *et al.* [17]. In these reports, the local stoichiometry of aggregates of individual molecules can be observed up to a degree of precision. However, the control experiments have yet to be performed to indicate if photophysical (quenching) or just physical interactions occur between individual fluorescent proteins.

However, the artificial system control experiment was performed with the relatively small fluorophore tetramethyl rhodamine (TMR) and with a relatively long linker. Considering that the live cell stoichiometric analysis was performed with the fluorophore eYFP fused to the L-type Ca^{2+} channel, a fusion protein that is five times larger than the eYFP fluorophore yet many times smaller than the diffraction limit, the chance that aggregation occurring from the observed affinity of eYFP towards dimerization and also the possibility of excited state interactions due to the close proximity of two fluorophores is low. There exists though the high possibility of natural

dimerization and also for excited state interactions to deem that the same control experiment has to be performed with the fluorescent protein [18].

An alternative to FRET is the pure co-localization of two spectrally different fluorophores. From the determination of position at the sub-resolution levels, it is possible to determine the distance of two different fluorescence emitting fluorophores down to a few nanometers limited most significantly by the signal and background levels [19,20]. As reported for large-scale experiments, a few different combinations of fluorescent proteins can be used for FRET other than the standard cyan fluorescent protein and yellow fluorescent protein. However, at the single-pair level, one combination of the yellow fluorescent protein and further red-shifted fluorescent proteins seemed promising and was first reported in 2000 [21]. Despite some drawbacks due to the oligomerization and aggregation of the DsRed in fusion protein constructs, the superior spectral separation between the yellow and red emission and the higher photostability of the donor (YFP) makes the YFP and DsRed FRET pair less ambiguous than the cyan and yellow FRET due to multitudes less of donor/acceptor bleedthrough and less donor photobleaching. Thus, in our attempt to obtain better information about the single-molecule possibilities, we tested the following combinations: F46L YFP and mRFP1 and also F46L YFP and eq611fp.

This type of experiment is fairly ubiquitous in many single molecule experiments but almost exclusively for pairs of artificial fluorophores such as Cy dyes, TMR, and Alexa dyes [22–26]. To date with the exception of one published experiment of the pure spFRET between two fluorescent proteins of CFP and YFP [27], the experiment has been described as impossible due to reported rapid photobleaching from the donor CFP at the single-molecule level [28,29]. The CFP variant has been reported by the same sources as producing such a low number of photons that it is not possible to image single molecules over statistical noise and background even under the best of conditions [30,31].

In this article, we will show the superiority of two fluorophores, the F46L YFP and the eqfp611 and also introduce the possibilities of using the mRFP fluorescent protein variant all at the single-molecule level. The means to show this is through various photophysical methods at the single-molecule level including saturation intensity, excitation/emission rate, and photobleaching statistical analysis; stoichiometric analysis to show dimerization and homotransfer and quenching trends; and co-localization and spFRET analysis for possibilities of new co-localization and FRET pairs. It is our intent to show this for future reference to observe cell signalling interactions in living cells at the single molecule level.

EXPERIMENTAL

Cloning, Expression and Purification of Fluorescent Proteins

The plasmid containing the EYFP coding sequence was obtained from BD Biosciences Clontech (Heidelberg, Germany). The F46L mutation was inserted into the EYFP sequence by PCR (Vilardaga *et al*., 1995), and its sequence was verified by dideoxy sequencing. A plasmid encoding mRFP1 was generously provided by Roger Y. Tsien. The plasmid for the eqfp611 was generously provided by Uli Nienhaus and Jörg Wiedenmann.

For the construction of bacterial expression plasmids, the open reading frames of EYFP, eYFP-F46L, mRFP1, and eqfp611 were amplified by PCR and simultaneously tagged with His_6 at the N-terminus. The resulting constructs were cloned into pET3a (Novagen). Sequences were verified by dideoxy sequencing.

For protein expression, *E. coli* BL21(DE3) (Novagen) were transformed with each of the expression plasmids. Fluorescent colonies were selected and grown in LB medium overnight at 37°C. On the next day, 500 mL of LB medium were inoculated with 5 mL of the overnight culture and grown to an optical density of 0.6–0.8 at 30°C. Cultures were then induced with 0.5 mM IPTG and grown for a further 3–6 hr before harvesting the bacteria. The bacterial pellets were resuspended in 20 mL PBS (phosphate buffer saline, 100 mM NaCl, 10 mM NaH_2PO_4, pH 7.5), and the suspension was stored at −20°C.

For protein purification, the bacteria were thawed and lysed on ice by sonication. Cell debris was removed by ultracentrifugation, and proteins were purified from the supernatant by affinity chromatography on nickel agarose (Qiagen, Hilden, Germany) according to the instructions of the manufacturer. Purification generally resulted in fluorescent proteins that were >90% pure as assessed by SDS polyacrylamide gel electrophoresis on 15% gels stained with Coomassie Blue and migrated at the expected molecular weights. The photophysical properties of both fluorescent proteins agreed well with previously published values for peak absorption, excitation and emission (see Table I). The protein samples were assayed spectrophotometrically by absorption on a Pharmacia Ultrospec 4000 (Germany) spectrophotometer. Excitation and emission spectra were measured on a Perkin-Elmer LS50B (USA) fluorimeter. Alexa 647 HNS ester and maleimide were

Table I. Photophysical Properties of Investigated Fluorophores

	λ_{exc} (nm)	I_s (kW cm^{-2})	k^{∞} (photons ms^{-1})	τ_{bl}^{∞} (ms)	ϕ_{bl} (10^{-5})	q
eYFP**	514	6.4 ± 0.5	3000 ± 200	3.2 ± 0.5	3.0 ± 0.6	0.13
eYFP-F64L	514	7.2 ± 0.7	3800 ± 200	8.5 ± 0.8	1.1 ± 0.1	0.05
DsRed**	532, 558	42 ± 12	++	++	++	++
mRFP1	573	27.2 ± 7.2	3300 ± 300	1.5 ± 0.5	5.1 ± 0.1	0.18
eqfp611	532, 558	4.9 ± 0.9	1900 ± 200	8.0 ± 0.8	0.66 ± 0.05	0.01
Alexa 647	635	4.0 ± 0.4	7100 ± 400	60 ± 10	0.021 ± 0.007	0

**Values re-checked and in agreement with Harms *et al*. (2001).
++ impossible to determine due to aggregation—see text.

purchased from Molecular Probes and dissolved in either methanol or PBS.

Gels

Polyacrylamide gels were made to 5% (w/w) with a purified stock solution of 30% acrylamide/1% bis-acrylamide added to 0.1% TEMED and a diluted solution of purified fluorescent protein. The gels were polymerized after addition of 0.1% of the APS catalyst in a thin smooth layer on cleaned #1, round glass slides of either 24 or 25 mm diameter (Fisher Scientific, USA and Assistant, Karl Hecht, Germany). The cleaning procedure is listed in the next section.

Films and Spin Coating

Samples were imbedded in poly vinyl alcohol (PVA, Roth Chemicals, Germany) films on cleaned glass slides by first spin coating 50 μL of a 1% solution of PVA in either ethanol (Appli Chem, Germany) or PBS on a spin coater (SPI, KW-4a, PA, USA) in two stages: for an initial period of 10 s at 300 rpm and then for 1 min at 2,000 rpm. Low concentrations of the fluorophores were either in the PVA solution or were spin coated in the prepared PVA film. Confocal microscopy of such films showed an average thickness of 1 μm.

Phospholipid Membranes

Lipid mixtures of DPPC (1,2-dipalmitoyl-sn-glycero-3-phosphocholin) (Avanti Polar Lipids, Alabama, USA) and *N*-(biotinoyl)-1,2-dihexadecanoyl-*sn*-glycero-3-phosphoethanolamine, triethylammonium salt (biotin DHPE) (Molecular Probes, Netherlands), were made by dissolving the pure lipids in chloroform. Two methods of creating supported membrane lipid bilayers on cleaned glass coverslips were used, Langmuir–Blodgett and vesicle fusion. Both methods produced nearly identical results. In both cases the glass coverslips were cleaned in 10% NaOH (AppliChem, Germany) solution with sonication for 10 min and then rinsed in 18 M Ohm water (Millipore, USA). For the Langmuir–Blodgett deposition, the lipid solution in chloroform (4 mg mL^{-1}) was deposited on the surface of a filtered phosphate buffer saline (PBS, 100 mM NaCl, 10 mM NaH_2PO_4, pH 7.5) solution in a monolayer trough (KSV, Minitrough, Finland). Addition of the lipid was made to a pressure of 5 mN m^{-1} and then compressed over 3 min to 30 mN m^{-1}. The first lipid monolayer was deposited by vertically pulling the glass slide substrate from the air/water surface of the trough with a velocity of 5 mm min^{-1} under constant pressure conditions. The substrate was immediately following re-deposited horizontally to the surface of the monolayer enriched trough. This substrate was then lifted into a perfusion chamber (Bioptechs, USA) in a manner so that it was always kept wet and never exposed to air. For vesicle fusion onto a glass support, the method of Snel *et al*. [32] was followed using lipid solutions that were dissolved in filtered phosphate buffered saline (PBS) to a final concentration of 2–5 mg mL^{-1}, sonicated, and deposited on to the cleaned substrates. Before incubation with a 50 nM solution of XFP-his_6 proteins the samples were incubated with 50 nM streptavidin (Sigma) and biotin-NTA (Molecular Probes, Netherlands), and then charged with a 5 mM Ni^{2+} for several minutes. In some cases, a mixture of 25 nM Biotin-NTA and 25 nM biocytin Alexa 647 (Molecular Probes, Netherlands).

Single-Molecule Imaging

The experimental arrangement for single-molecule imaging has been described in detail previously [22,33,34] (see also Fig. 1). Essentially, the samples were mounted onto an inverted microscope (Zeiss, Axiovert 200) equipped with a 100× objective (NA = 1.4, Zeiss), and illuminated for 1–30 ms by an Ar^+-laser (Coherent Innova 308) and dye laser (Coherent, CR-599) synchronized with the exposure of the peltier-cooled CCD-camera system

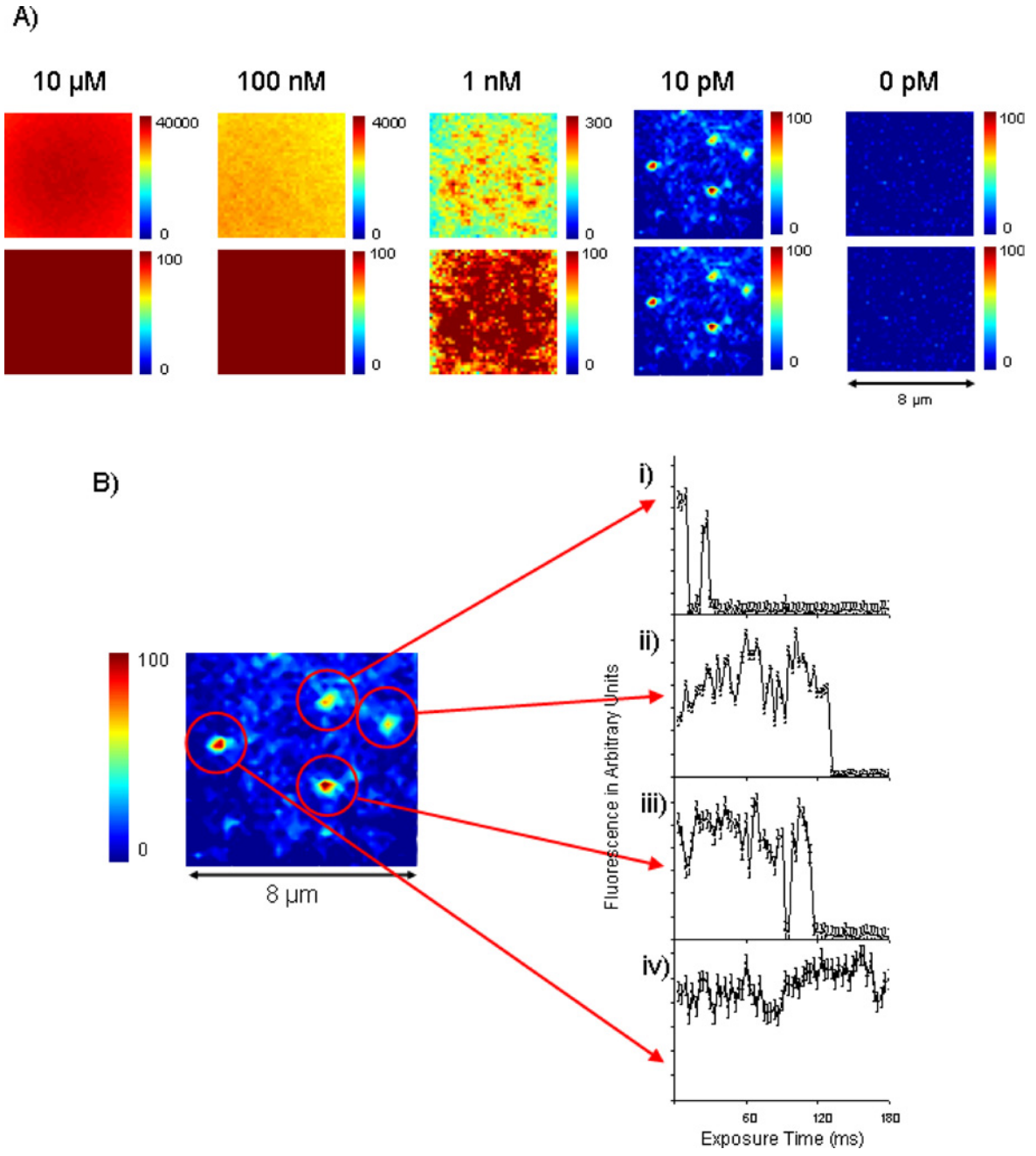

Fig. 1. (A) Fluorescence images of different concentrations of F46L YFP in a PVA film on a coverslip. *Upper row*: scaled to show the full intensity range of each image; *bottom row*: scaled to the level where single molecules are observed. All images were recorded at 3 kW cm^{-2} for 3 ms. (B) Time trajectories of four individual F46L YFP's (i–iv) from the single molecule image (*left*). The image is non-standard because the most typical results for this molecule is represented by (i) which lasts for 15 ms in the on-state and blinks (i.e., turns on and off one time). Two molecules (ii) and (iii) lasted much longer than average. A fourth molecule (iv) never photobleached during the integration period but has the same fluorescence emission rate as the other three. (for color figure, see online version).

(Spec-10, 400B or 1300 B, Roper Scientific). The synchronizazion was by the use of home-built electronics to set the exposure trigger from the CCD camera and a shutter—either an acousto-optic time-frequency shutter (AOTF, AA Optic, France) or an ultrafast mechanical shutter (nm Laser, CA, USA)—to control the laser light excitation. The single fluorescent proteins are best detected with the proper filter combinations: (DCLP525 and HQ570/80

(Chroma, VT, USA) for eYFP and eYFP-F46L; DCLP575 and HQ620/80 (Chroma, VT, USA) for mRFP1, DsRed, and eqfp611; DCLP580 (Chroma, VT, USA)and OG590 (Schott, Germany) for mRFP1; DCLP595 (Chroma, VT, USA) and RG610 (Schott, Germany) for eqfp611; DCLP 580, HQ600/80; DCLP525, HQ570/80M (Chroma, VT, USA), and OG530-3 and OG590-3 (Schott, Germany) and custom dual-color filters and wedge filters (or appropriate color image separator, unpublished result) for sYFP/eqfp611 and for eqfp611/Alexa647 (custom design, Chroma, VT, USA) allowed the detection of the individual fluorescent proteins and also single pair fluorescence resonance energy transfer detection by the peltier-cooled CCD-camera systems with camera quantum efficiencies of >90%. The total detection efficiency of the experimental setup was 10% for eYFP and eYFP-F46L, 16% for DsRed, 16% for mRFP1, 7% for eqfp611, and 14% for Alexa 647. The photon counts were determined with a precision of $\sim>\pm 15\%$. Data processing occurred in methods similar to Harms *et al*. [33, 34, 36] with self-made programs in Matlab (Math Works, USA).

Stoichiometric Determination and FRET Analysis

Given that the measured single-molecule intensity is described by a probability density function $\rho_1(\mathrm{I})$ with a mean of I_1 and with of σ_1 counts, the intensity of N independent, fluorescing molecules of the same kind are described by the convolution integral:

$$\rho_N(i) = \int dI' \rho_1(I') \rho_{N-1}(I - I')$$

yielding a mean of $I_N = N \times I_1$ and $\sigma_N = N^{1/2} \times \sigma_1$ [35,36].

To test the level of interaction from individual fluorophores a simple test was carried out on the single-molecule signal level to bring a statistical number of fluorophores in small (hot spots) localized regions in a method similar to Schmidt *et al*. (1997). The creation of the samples started with the attachment of avidin or streptavidin to a support (either a membrane bi-layer or directly by tethering to a coverglass—in buffer). Then biotin NTA (100 nM) was flowed followed by a charge of Ni^{2+}. At this point the fluorescent proteins were flowed in and washed several times with buffer. To ensure that binding was specific to Ni^{2+} NTA groups, solutions of EDTA were flowed and washed while imaging the fluorescence during this process. The specificity of the interaction during the addition, removal, and re-addition of fluorescent proteins was observed where the spots of fluorescent binding remained consistent during the addition/removal cycles.

For FRET imaging, a dual color filter set (custom sets from chroma—for sYFP and eqfp611 dichroic mirror and band pass emission filter with detection efficiency 9.8%—YFP and 13.1%—eqfp611 in their respective channels with crosstalk of 0.01% of YFP in the eqfp611 channel and 0.08% of eqfp611 in the YFP) was used and the emission light was split by a dual color wedge to yield two images on the CCD camera as described previously [22,37]. The detection efficiency was determined and also calculated to be for the case of YFP and eqfp611, 9.8% and 13.1%, respectively and for the case of eqfp611 and Alexa 647, 8.9% and 6.4%, respectively. By this method and additionally toggled excitation between donor and acceptor wavelength, it was possible to measure the level of FRET occurring and, a few milliseconds later, check for the presence of acceptor in exactly the same spot. From control experiments of just the one type of fluorophore alone, there was never any observed cross-talk or bleedthorugh detectable beyond the noise of the CCD cameras in agreement with the determined <0.01% crosstalk and bleed through for the YFP and eqfp611 experiment and <0.1% for the eqfp611 and Alexa 647 experiment. To determine the level of FRET, the individual peaks in each color channel were fitted by a two-dimensional gaussian function to determine position and intensity. The FRET efficiency reported is the ratio $(1 + \frac{\eta_\mathrm{A}}{\eta_\mathrm{D}} \frac{\phi_\mathrm{A}}{\phi_\mathrm{D}} \frac{F_\mathrm{D}}{F_\mathrm{A}})^{-1}$ with η_A and η_D as the detection efficiencies, ϕ_A and ϕ_B as the quantum efficiencies, and F_A and F_D as the determined fluorescence signal of the acceptor (A) and donor (D) [22].

RESULTS

Single Molecule Characterization of F46L YFP, mRFP1, eqfp611, and Alexa 647

Amongst the various methods to describe the fluorescent proteins, we still consider the previously reported method from Harms *et al*. [38], but we have gone further in depth to consider more fundamental photophysical effects. Briefly, the fundamental steps of the characterization is to determine that we are observing single molecules of a particular fluorophore (and what percentage is fluorescing at a given time), to identify the emission rate at defined excitation for the average molecule, thus the average number of photons one can expect per molecule and finally environmental effects.

First, we determined for all samples the concentration needed to apply on a coverglass to observe single molecules. The appropriate concentration level of the single molecules could be checked by many standards previously reported in the literature and remains with a factor of error for the pure difficulty of determining concentration

at very low levels quite consistent, but within an order of magnitude. Figure 1 shows images of auto-scaled fluorescence with decreasing concentration (left to right) of the yellow fluorescent protein (F46L YFP) under investigation in this study. The bottom images are the same scaled at the fixed level of the single molecule level measurements.

It is at these low concentrations (Fig. 1) where the interesting phenomena such as the single-step photobleach, the well-aligned dipole, and photon bunching and antibunching occur [39,40]. This is also where our investigation begins. Understanding the phenomena and simply the photoresponse of different fluorophore types so that the ultimate goal of observing individual fluorophores in specific environments—in this case attached to proteins in different organelles of living cells, tissues, and organisms—can be stabily and reliably achieved.

Signal Levels, Saturation Intensities, and Photobleaching Behavior of Autofluorescent Proteins In Vitro

Although many single molecule reports exist entirely on the prospect of finding subtle differences of the fluorophores from time-traces of the single-molecule fluorescence behavior, we find that for wide-field single molecule imaging it is most useful to report the standard emission rate behavior and appearance and kinetics of photophysically and photochemically active dark states versus the excitation rate to determine the saturating point of the maximum emission rate by the same instrument that will be used for single-molecule tracking and single-pair colocalization measurements. The individual molecules that are observed by the integrated image are then tracked by each consecutive image until the molecule reaches a dark state and stops emitting fluorescence. In the majority of cases, the fluorescence does not re-appear. This is photobleaching. In a minority of cases, the fluorescence does reappear. This is blinking. Because we are mostly only interested in the fluorescing state, we describe the photobleaching time as the time during the exposures that the molecule was fluorescing. We describe these basic photophysical parameters of the autofluorescent proteins by the saturation intensity, I_s, the photobleaching time-limit at infinite excitation intensity, τ_{bl}^{∞}, and the maximal photon emission rate k_{∞}. In addition to single-molecule experiments, we compare and re-inforce all single molecule results with high-concentration—greater than 50 nM—sample results. In this way we understand for single molecule tracking and co-localization experiments the average of what we can expect from a single fluorescing molecule and also the upper limit of the occasional molecule that is stable for longer periods.

Histograms of the averaged individual molecule fluorescence emission intensity, $\langle F \rangle$ and the on-time to photobleach, $\tau_{bl,}$ (bl = 15 ms in the example in Fig. 1B(i) at individual excitation intensities were produced to obtain the statistics and standard error of the individual data points of the fluorescent proteins eYFP, DsRed, F46L YFP, mRFP1, eqpf611, and Alexa 647 in both polyacrylamide gels or in poly vinyl alcohol spin coated films. The fluorescence intensity histogram is interpreted by probability distribution analysis and is nearly a Gaussian distribution with mean and standard error extracted for further analysis. The on time to photobleach statistics are described by a single exponential decay $\propto e^{-t/\tau bl}$ and is first order as the model for photobleaching is due to first order kinetics of the chemical reaction with oxygen to create a photobleached state. There are some molecules that last longer orders of magnitude longer (Birks, Turro).

The fluorescence signals, converted to the rate of photon emitted by the detection efficiency, and the time-to-photobleach signals are mapped out versus the respective excitation intensity. Such a mapping should report the parallel information about expected maximum fluorescence emissions and on-time-to-photobleach that are both saturation limited from the excitation rate and should follow from models of level photophysics with the definition

$$\begin{aligned} S_{det}(I,t) &= \frac{\eta_{det} k_{\infty} t}{1 + I_s/I}; \quad F(I) \\ &= \frac{S_{det}}{\eta \det \tau_{bl}(I)(1 - \exp(-t/\tau_{bl}(I))} \\ &= \frac{k_{\infty}}{1 + I_s/I}; \quad \text{and} \quad \tau_{bl}(I) = \tau_{bl}^{\infty}(1 + I_s/I) \end{aligned}$$

(where S_{det} is the detected signal, F the photon emission (fluorescence) rate, I_s is the saturation intensity and k_{∞} is the maximum emission rate at infinite excitation, τ_{bl}^{∞}, the time it takes the fluorophore to undergo photobleaching at infinite excitation intensity) as long as the fluorescence signal data recorded does not involve integration times that might also include large periods of photobleach [41]. In such cases of large photobleaching, either little or no signal can be observed (meaning that detection of the single molecule is not possible) or a correction can be used [42] which was only necessary to apply in the case of the mRFP (with the previously reported photobleaching rates for mRFP, this is not surprising and will be examined in the discussion section later). The values for I_s, k_{∞}, and τ_{bl}^{∞}, were determined for various excitation intensities as shown in Table I for F46L YFP, mRFP, and Alexa647 in gel and in the film for excitation intensities between 0.1 and 60 kW cm^{-2} and for

illumination times between 0.5 and 30 ms from the data shown in Fig. 2A–H. Additional fluorescence correlation spectroscopy (FCS) and time-correlated single photon counting of sYFP in polyacrylamide gels (data not shown) were done. The mutual dependence on the photobleaching time with excitation intensity is clearly visible. The data in Fig. 2A–H follow the predicted behavior yielding the photobleaching time limit of 1.5 ± 0.5 ms for mRFP and for in gel and film and some interesting longer time behavior for Alexa 647 with $\tau_{bl}^{\infty} = 60 \pm 10$ ms, for sYFP with $\tau_{bl}^{\infty} = 8.5 \pm 0.8$ ms, and for eqfp611 with 8.0 ± 0.8 ms. As can be seen the photobleaching times for the fluorescent proteins are about 10 times faster than those reported for synthetic fluorophores typically used in single-molecule research (in this case of the Alexa 647). The saturation intensities for the mRFP and the F46L YFP are also found to be similar to their structural neighbors of the DsRed and eYFP [43].

We have first of all observed that for some samples, the F46L YFP, the eqfp611, and the Alexa 647, that the quick occurrence of dark states or of photobleaching during the first imaging period did not on-average occur. Comparing the different autofluorescent proteins, the results detailed above are summarized in table 1. The maximum emission rate varies from $k_{\infty} \sim 1500$ for eqfp611 to 6900 photons ms^{-1} for Alexa 647, the saturation intensity varies between 4 and 42 kW cm^{-2}, and the photobleaching times varying between $\tau_{bl}^{\infty}=$ to 3.5 ms in aqueous environments, at pH 7.4, and at ambient temperatures. From the values it appears that the suitability of the autofluorescence proteins for single-molecule microscopy is given by eqfp611 $\sim$ F46L YFP > eYFP > eGFP $\gg$ eCFP, leaving DsRed once again out of consideration. A detailed evaluation of that ranking will be specified in the discussion section. Thus, we find that the two tags eqfp611 and F46L-YFP are more suited for attempts of observing single fluorescent fustion proteins at cell surfaces.

Signal Level and Stoichiometry of Bound eYFP

Co-Localization and spFRET Signal Level from F46L YFP, mRFP, eqFP611 and Alexa 647

We were interested in testing the fluorescent proteins for their behavior when artificially placed in stoichiometric clusters and in a method comparable to other fluorophores. We used biotin-strepatavidin system a fluorescence labelled biotin streptavidin system (see materials and methods). As this control method and analysis have been previously reported for a TMR labeled biotin and analysis has been used for clusters of single molecules on surfaces of cells, we can use this as a comparative model.

From the resulting distribution of intensities of the methods for each of the fluorescent proteins as shown in Fig. 3, stoichiometries can be determined by assigning a peak with a certain intensity a number of fluorescing molecules according to Schmidt *et al*. (1996) [44]. From the statistical calculation of the correct distribution, a binomial distribution, of random binding with equal affinity resulted in a ratio of streptavidin:biotin 1:1 with 26%, 1:2 with 40%, 1:3 with 26%, 1:4 with 7%. With a perfect fluorophore for such stoichiometric calculation, one would assume that the fluorophores do not interact both physically by affinity or repulsion or photophysically by possible electronic interactions of the fluorophore excited state.

From the application of the individual fluorophores to this stoichiometric test some predictable behaviour was immediately observed in that the distribution favored a near perfect binomial behaviour for Alexa 647 and that the DsRed showed an enormously different behaviour to the norm in that a heavily larger distribution of more fluorophores was observed in a single diffraction limited hot spot. Both distributions have precedents in the literature. Alexa dyes show no major affinity to aggregrate or electronically interact for such an average molecular distance. The DsRed forms natural tetramers and thus changes the appearance of the binding stoichiometry to on average 4–16 fluorophores.

In the other cases we determined the probability distribution from histograms and performed least-squared fitting analysis of Gaussian functions for placement and size of the individual higher probability distributions (or subset of events). Figure 3 shows the histograms, probability distribution, and multiple Gaussian fit. For each of these distributions we compare the control data of peak maxima of convolution of the pure single-molecule control data to the Gaussian fitting results. A straight line $I_N = N \times I_1$ with I_N being the detected fluorescence intensity of a cluster of N molecules represents the absolute expected fluorescence. The Gaussian fit data represents the measured case, where a number of fluorophores might interach and thus suppress or quench fluorescence. If we apply this data to the Stern–Volmer model of quenching $I/I_0 = 1 + q \times [Q]$, and replace the expected fluorescence without quencher F_0 by N times the intensity of a single molecule I_1 and at the same time the quencher concentration $[Q]$ by the number of additional molecules that might reduce the emission (as we show graphically for eYFP, mRFP, F46L YFP, and eqfp611 in the insets of Fig. 3), we can derive the pure single-molecule level equation for quenching:

$$I_N = N \times I_1/(1 + (N - 1) \times q)$$

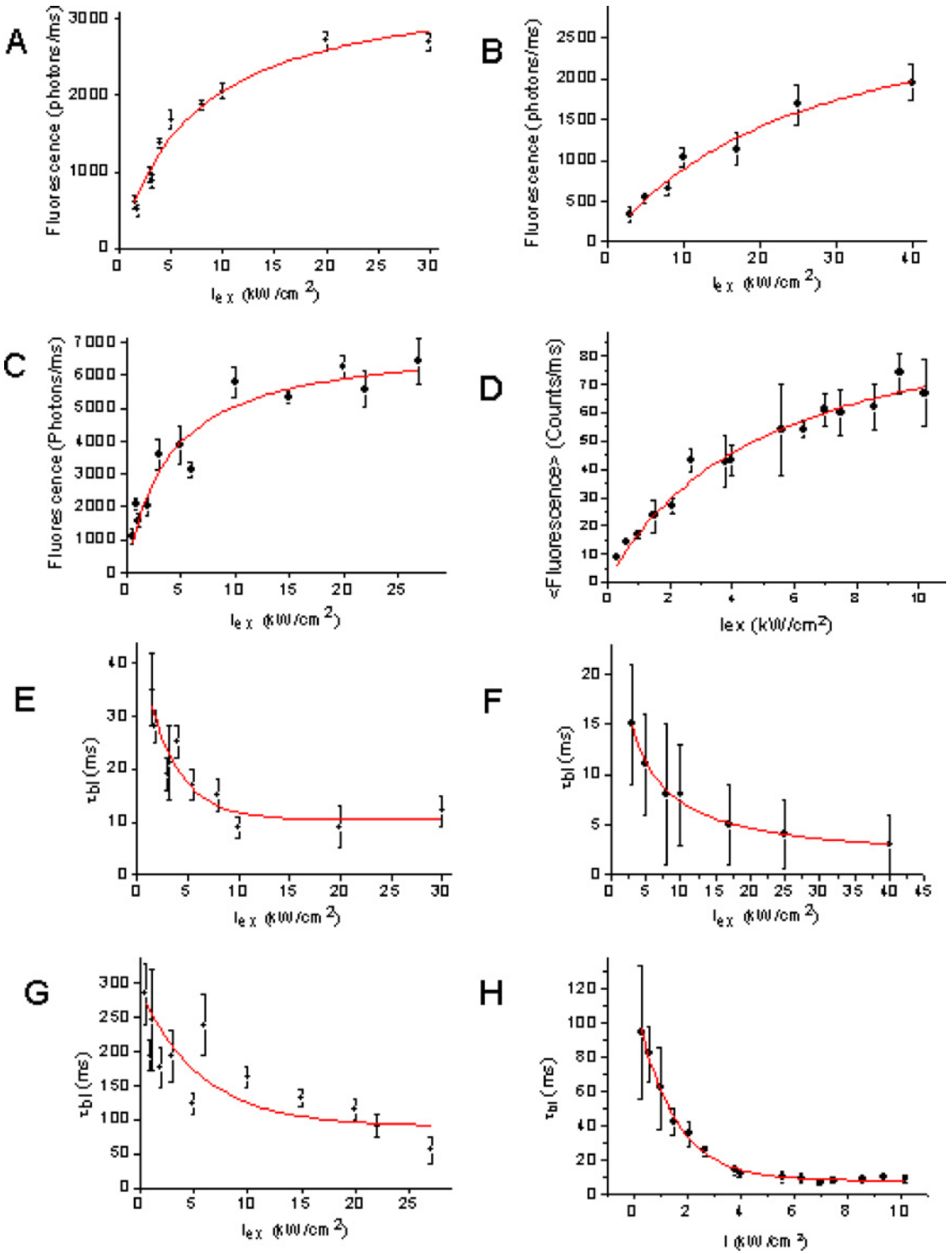

Fig. 2. Saturation curves for the single molecule fluorescence emission rate (photons ms^{-1}) as function of the excitation intensity. (A) sYFP: $I_s = 7.2\,kW\,cm^{-2}$, $k_\infty = 3800$ photons ms^{-1} (B) mRFP: $I_s = 27.2\,kW\,cm^{-2}$, $k_\infty = 3300$ photons ms^{-1} (C) Alexa647: $I_s = 4.0\,kW\,cm^{-2}$, $k_\infty = 7100$ photons ms^{-1} (D) eqfp611: $I_s = 4.9\,kW\,cm^{-2}$, $k_\infty = 1900$ photons ms^{-1}, and bleach times as a function of the excitation intensity—the bleach times for infinite excitation intensities differ between the three fluorophores shown: (E) eYFP: $\tau_{bl}^{\infty} = 3.2$ ms (F) mRFP: $\tau_{bl}^{\infty} = 1.5$ ms (G) Alexa647: $\tau_{bl}^{\infty} = 60$ ms (H) eqfp611: $\tau_{bl}^{\infty} = 8.0$ ms.

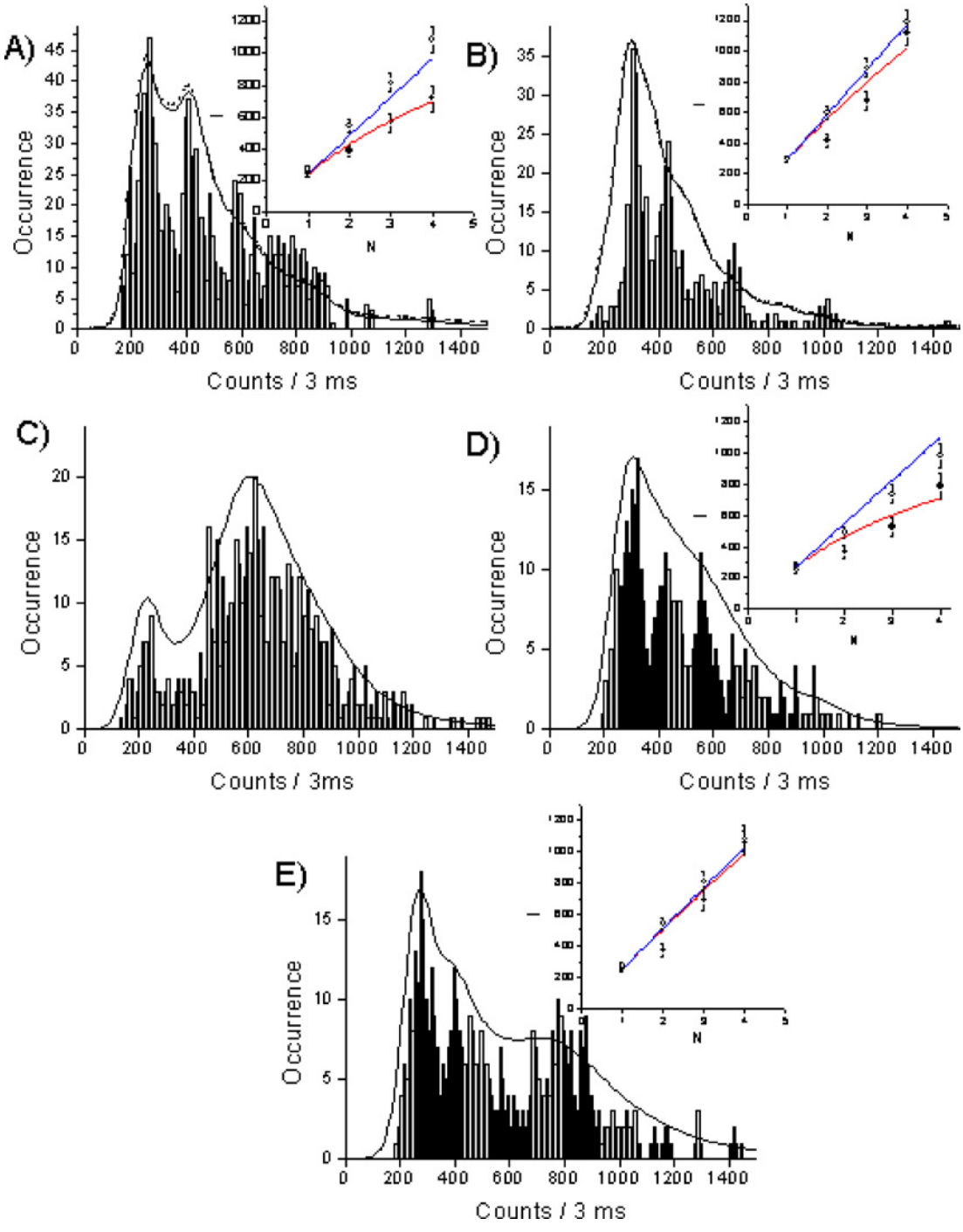

Fig. 3. Distribution of intensities from diffraction limited spots in experiments (for 3 ms each at $0.8 \times I_s$ kW cm^{-2}): (A) eYFP (B) F46LYFP (C) DsRed (D) mRFP (E) eqfp611 Measured data is shown in bars, fit with a sum of gaussian curves where the most probable values for clusters of single molecules. Insets to all Fig. (A)–(E): Expected stoichiometry signal and quenching graph. The single molecule control experiment times the stoichiometry number were estimated in open circles with error and curve shown with a blue line. The actual result of the experiment from the Gaussian distribution peak fit is shown with standard error bar by the dark circles. The red line shows the fit to the stoichiometry equation (see text) from the quenching parameter q was determined. (for color figure, see online version).

We find from our model we can attribute the quenching to the fitting factor "q" and that the mRFP and eYFP show a significant quench with $q = 0.18$ and 0.13, respectively, and that the sYFP and the eqfp611 show extremely small levels of quenching (see values in Table I), $q \leq 0.05$. We will attribute the level of quenching and ramifications in the discussion section.

As a complement to local stoichiometry, the possibility of spFRET occurring between two fluorescent proteins or with even one fluorescent protein as either donor or acceptor has resulted in few successes in the field of single-molecule imaging or spectroscopy. The aforementioned reasons for this are the poor stability in one of the fluorescent protein variants (generally the eCFP) or high autofluorescence that limits the use of the fluorescent proteins. In general, the reason is the limited fluorescence of the fluorescent proteins that does not always allow them to be observed in vivo.

From our above determination that two fluorophores seem to be superior above the others, the sYFP and eqfp611, in terms of low photobleaching and high signal, we attempted to test them for the possibility of FRET. From spectral overlap predictions and assuming random orientations of the fluorophores ($\kappa^2 = 2/3$) (in water $n = 1.33$), the Förster distance (the distance at which 50% energy transfer occurs) between these fluorophores (the F46L YFP and eqfp611) is 6.7 nm. This is clearly superior to the estimated 5.2 nm for the combination of eCFP and eYFP and not accounting for the lower instability of the eCFP fluorophore.

Furthermore, an even greater spFRET pair exists when we were to use the artificial fluorophore of Alexa 647 as an acceptor for the donor fluorescent protein, eqfp611. In this case and under the same assumptions, the Förster radius is 8.0 nm, the fluorophore brightness and stability is superior to any other combination used in this article, and the fluorescence emission is best separated between donor and acceptor with the fewest hindrances due to flavin autofluorescence for in vivo experimentation.

For our tests, we use the same underlying principle of attachment of biotinylated fluorophores either with Alexa 647 biocytin (Molecular Probes) or the same Ni^{2+}:NTA biotin that attaches directly to the his_6 groups on the fluorescent proteins. With the addition of the fluorophores, some of the hotspots showed signals that responded to a presence of both the donor and acceptor molecules being present. The signals could be specifically controlled by excitation and/or be emission separation: for example, excitation with 488 nm of the sYFP for 5 ms and at 3 kW cm^{-2} resulted in only emission detection of single sYFP in the "yellow channel" while the excitation conditions at 560 nm for single eqfp611 resulted in only emission detection in the "red channel." The presence of a FRET signal was concluded when 514 nm excitation resulted in a signal in the "red channel" and could be verified by presence of acceptor with excitation at 560 nm. An example of a sp FRET trajectory in this case, is shown in Fig. 4A.

The control was even better between excitation and emission with the eqfp611 and the Alexa647 spFRET pair. The emission signal of eqfp611 was specific to excitation at 560 nm at 3 kW cm^{-2} for 10 ms in the "orange" channel. The emission signal of Alexa 647 was specific for excitation at 632 nm at 3 kW cm^{-2} for 5 ms. For the pure components at the single-molecule level, the separation was perfect allowing us to determine a completely unambiguous FRET. With the aid of toggled excitation, for each case of FRET, when emission occurred in the red channel during excitation of the donor, we could determine the presence of the acceptor by excitation with 632 nm. An example of a sp FRET trajectory in this case, is shown in Fig. 4B.

Examples of each of these cases the signals of the individual channels were determined by the standard Gaussian fitting routines, and the FRET efficiency was determined for each case that resulted that appeared to have a significant level (see materials and methods). The average FRET efficiency was determined for each measurement and combined over a multiple number of individually separate co-localized areas for the creation of a FRET histogram. The histograms are shown in Fig. 4C and represent an average transfer efficiency of 0.46 ± 0.11 for F46L YFP/eqfp611 and 0.72 ± 0.15 for eqfp611/Alexa647 individually separate FRET measurements. We will attribute the level of FRET, the future applications and ramifications in the discussion section.

DISCUSSION

A proverbial question occurs in single-molecule detection in cells of which fluorophore—in this case which fluorescent protein—is best. The answer can be understood by carefully dissecting the properties of the fluorophores versus the properties of the background. As mentioned, such a study already existed which drew a conclusion that the eYFP from the ratio of detection of the fluorescent protein to the detection of flavin background under the conditions of the protein detection. Naturally, the further red-shifted DsRed was discounted because it was suspect to heavy oligomerization and could not be used practically in fusion constructs at the single-molecule level.

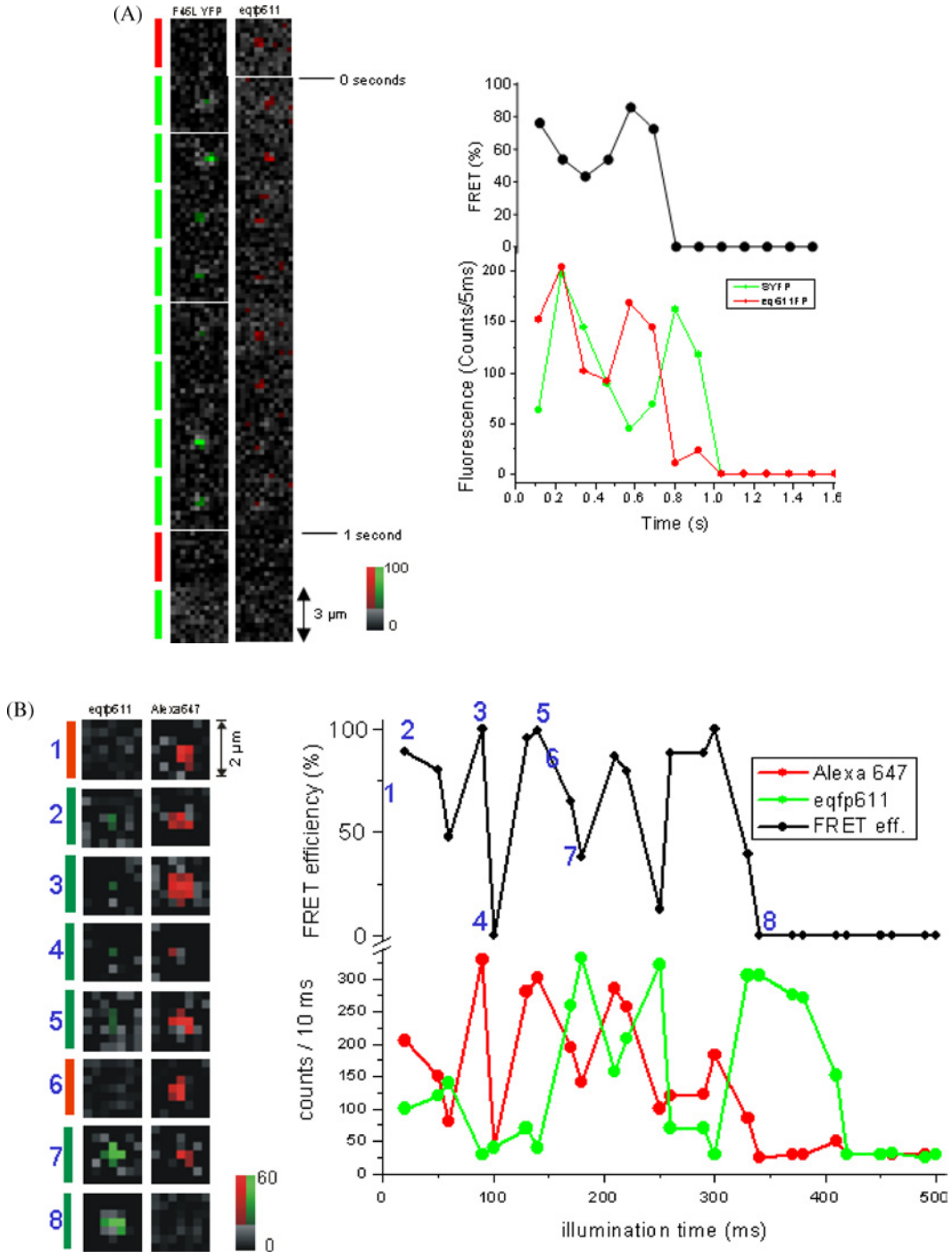

Fig. 4. (A) Single molecule FRET observations with sYFP and eq611fp. The *left panel* shows images in the two channels, the graphs on the *right* show the FRET ratio ($I_{\mathrm{eq611fp}}/(I_{\mathrm{sYFP}} + I_{\mathrm{eq611fp}})$) (*top*) and the individual intensities (*bottom*). The *bars at the left* indicate the laser line used to excite the fluorophore. (B) Single molecule FRET observations with eq611fp and Alexa 647. The graphs show the calculated FRET efficiency (*top*) and the individual intensities in the peaks (*bottom*) shown as images in the right panel. Numbers in the FRET efficiency graph refer to the images, on the right that the values were calculated from. (C) Distribution of FRET efficiencies for the two fluorophore pairs tested. The average FRET efficiency of eq611fp/Alexa647 is about 1.8 times larger than for sYFP/eq611fp. (for color figure, see online version).

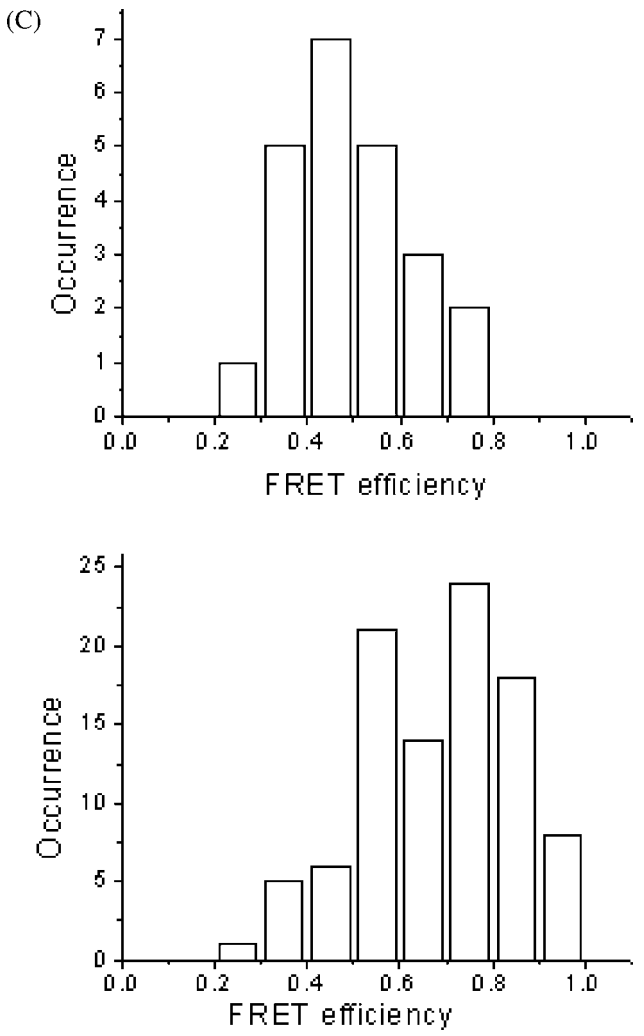

Fig. 4. Continued.

If we apply the original criteria [45] to the newly developed and tested fluorescent proteins, it is clear that there are two new recommendations: the F46L YFP and the eqfp611 with a third possibility of mRFP1.

The criteria of overall detectablility over background from the original method results in the parameter R [45], which roughly tells how many background flavin molecules could be present for a 1:1 signal:noise ratio and improves to $\gg 10^4$ for the eqfp611. The mRFP also results in a somewhat superior value, and the F46L YFP remains unchanged. However, this parameter, R, needs some adjustments for accounting of other cellular background fluorescence molecules such as myelin, and a relative stability parameter such as the photobleaching efficiency which would certainly favor the F46L YFP and disfavour the mRFP. Additionally, differences in saturation intensities should be considered since they cause the need of higher excitation intensity for some fluorophores and thus give rise for higher background fluorescence. The last parameter to consider is the degree of applicability of the fluorophore for such hindrances due to oligomerization and quenching. In this way, with the complete results of our study including the stoichiometry and quenching vaules, we could have a qualitiative modified R_{mod} value to show the relative strengths of the fluorescent proteins to be (from best to last in order) eqfp611 > F46L YFP > mRFP.

We are not surprised to yield such results as it was possible to predict that we must have some type of superior behaviour from all of these proteins. First, from bulk rate measurements it could be predicted that saturation intensities and single molecule fluorescence emission rates would be higher, which was confirmed by our observations yielding saturation intensities I_{s} of $3\,\mathrm{kW\,cm^{-2}}$ for eqfp611 (using the suggested emission scheme from

Schenk *et al*. 2004 [46]), 16 kW cm^{-2} for F46L YFP and 60 kW cm^{-2} for mRFP (using the five level system scheme and rate values from Nagai [47] and from Campbell [48]). The maximum emission rates were 2000 photons ms^{-1} for eqfp611, 6000 photons ms^{-1} for F46L YFP and 5000 photons ms^{-1} for mRFP. Second from previously published bulk photobleaching rates and brightness phenomena, we could estimate that eqfp611 and sYFP should be some 2–20 times more photostable than the eYFP and that the mRFP should be less photostable. Lastly, from bulk oligomerization studies and also brightness phenomena, we could predict local stoichiometry and quenching to be superior for all three of these fluorophore.

It is interesting that for F46L YFP a greater photostability was observed in that the single-molecule photobleaching was less with an average photobleaching time three times larger than eYFP. This was also complemented in the observation that the quenching of the single molecules is less from the stoichiometry control experiment than eYFP. We therefore suspect that the observed improved 20-fold fluorescence [49] is an effect that occurs in higher expression systems because of reduced photobleaching and lower quenching. The effect of longer maturation helps only in the case of FRET partners and is a reason below to use F46L YFP as a single-pair FRET partner.

The possibility of being able to observe spFRET between two fluorescent proteins and also for this combination in living cells is very promising. The combination of F46L YFP and eqfp611 seems to be quite feasible although the average transfer efficiency of 0.46 ± 0.11 does not appear high. Considering the detection efficiency, the non-modified detection ratio, the photobleaching rate, and off rate for this pair, it is estimated that for a definite FRET one spFRET in four will be detected. Considering the impossibility of detection for other fluorescent protein pairs, our intent is to incorporate this into our reperatory of standard measurements for both co-localization of two proteins and for studies of protein conformational change.

The more recommended stable FRET pair for single molecule studies when only one partner must be a fluorescent protein is the combination of eqfp611 as a donor and Alexa647 as an acceptor. The large stokes shift between donor excitation and the donor emission as well as the well-separated acceptor emission plus spectral emission regions far from many background autofluorescent molecules in living cells make the high detectability with low bleedthrough an excellent combination for spFRET. The probability of detection of each spFRET pair in this case is nearly one in two.

Furthermore, we have also shown an example of the superiority of the artificial fluorophores in comparison to the fluorescent proteins for single molecule studies. At best, one would prefer not to use fluorescent proteins for single-molecule studies as they are generally less stabile and larger and bulkier and have a higher potential to alter the activity of the fused protein. In this article, we suggest that for single-molecule detection in living epithelial cells the best way to combat autofluorescence is through the use of red or infra-red artificial fluorophores (e.g., Alexa 647 or Cy5 or Cy7) because of the great photostability.

However, we have hope in the future for the use of the fluorescent proteins with the introduction of the newer variants since a similar initial report in 2001 [50]. We anticipate that with the advent of many new variants to come, there will be a need for constant updates on the recommendation for the use of the fluorescent proteins in single molecule studies. The advantage of the creation of new more red-shifted and photostabile autofluorescent proteins is that the most convenient way to correctly obtain a single fluorophore on a protein in the most natural environment is through the fusion of fluorescent proteins to specific target proteins.

We also hope to introduce new strategies for labelling artificial fluorophores for which new labelling mechanisms have been developed for gentler and easier labelling for in vivo applications and these applications will soon be developed for QDots (best of all) which have only been used with antibody labels—antibody labels lead to some non-specificity and clustering effects. All of these new methods provide us with improved methods and analysis for future studies with ion channels, growth factors, integrins, and GPCRs. We even hope that with such research, a new age will come when we speak of single-molecule tracking in living tissues.

ACKNOWLEDGMENTS

We thank Verena Schürger, David Panther, Geoffrey Lambright, Kira Gromova, and Gaby Wolz-Curtaz for their laboratory assistance during the course of this work. This work was supported by the German Science Foundation (DFG) Grant number FZT 82.

REFERENCES

1. T. Nagai, K. Ibata, E. S. Park, M. Kubota, K. Mikoshiba, and A. Miyawaki (2002). *Nat. Biotechnol.* **20**, 87–90.
2. R. E. Campbell, O. Tour, A. E. Palmer, P. A. Steinbach, G. S. Baird, D. A. Zacharias, and R. Y. Tsien (2002). *Proc. Natl. Acad. Sci. USA* **99**, 7877–7882.

3. T. Nagai, K. Ibata, E. S. Park, M. Kubota, K. Mikoshiba, and A. Miyawaki (2002). *Nat. Biotechnol.* **20**, 87–90.
4. R. E. Campbell, O. Tour, A. E. Palmer, P. A. Steinbach, G. S. Baird, D. A. Zacharias, and R. Y. Tsien (2002). *Proc. Natl. Acad. Sci. USA* **99**, 7877–7882.
5. G. S. Harms, L. Cognet, P. H. Lommerse, G. A. Blab, and T. Schmidt (2001). *Biophys. J.* **80**, 2396–2408.
6. G. S. Harms, L. Cognet, P. H. Lommerse, G. A. Blab, and T. Schmidt (2001). *Biophys. J.* **80**, 2396–2408.
7. A. Schenk, S. Ivanchenko, C. Rocker, J. Wiedenmann, and G. U. Nienhaus (2004). *Biophys. J.* **86**, 384–394.
8. K. Nienhaus, B. Vallone, F. Renzi, J. Wiedenmann, and G. U. Nienhaus (2003). *Acta Crystallogr. D. Biol. Crystallogr.* **59**, 1253–1255.
9. J. Wiedenmann, A. Schenk, C. Rocker, A. Girod, K. D. Spindler, and G. U. Nienhaus (2002). *Proc. Natl. Acad. Sci. USA* **99**, 11646–11651.
10. G. S. Harms, L. Cognet, P. H. Lommerse, G. A. Blab, and T. Schmidt (2001). *Biophys. J.* **80**, 2396–2408.
11. G. S. Harms, L. Cognet, P. H. Lommerse, G. A. Blab, H. Kahr, R. Gamsjager, H. P. Spaink, N. M. Soldatov, C. Romanin, and T. Schmidt (2001). *Biophys. J.* **81**, 2639–2646.
12. P. H. Lommerse, G. A. Blab, L. Cognet, G. S. Harms, B. E. Snaar-Jagalska, H. P. Spaink, and T. Schmidt (2004). *Biophys. J.* **86**, 609–616.
13. H. Murakoshi, R. Iino, T. Kobayashi, T. Fujiwara, C. Ohshima, A. Yoshimura, and A. Kusumi (2004). *Proc. Natl. Acad. Sci. USA.* **101,** 7317–7322.
14. F. de Lange, A. Cambi, R. Huijbens, B. de Bakker, W. Rensen, M. Garcia-Parajo, N. van Hulst, and C. G. Figdor (2001). *J. Cell Sci.* **114**, 4153–4160.
15. S. W. Hell (2003). *Nat. Biotechnol.* **21**, 1347–1355.
16. Th. Schmidt, G. J. Schuetz, H. J. Gruber, and H. Schindler (1996). *Anal. Chem.* **68**, 4397–4401.
17. G. S. Harms, L. Cognet, P. H. Lommerse, G. A. Blab, H. Kahr, R. Gamsjager, H P. Spaink, N. M. Soldatov, C. Romanin, and T. Schmidt (2001). *Biophys. J.* **81**, 2639–2646.
18. D. A. Zacharias, J. D. Violin, A. C. Newton, and R. Y. Tsien (2002). *Science* **296**, 913–916.
19. T. D. Lacoste, X. Michalet, F. Pinaud, D. S. Chemla, A. P. Alivisatos, and S. Weiss (2000). *Proc. Natl. Acad. Sci. USA* **97**, 9461–9466.
20. R. E. Thompson, D. R. Larson, and W. W. Webb (2002). *Biophys. J.* **82**, 2775–2783.
21. H. Mizuno, A. Sawano, P. Eli, H. Hama, and A. Miyawaki (2001). *Biochemistry* **40**, 2502–2510.
22. L. Cognet, G. S. Harms, G. Blab, P. H. M. Lommerse, and Th. Schmidt (2000). *Appl. Phys. Lett.* **77**, 1–3.
23. G. S. Harms, G. Orr, M. Montal, B. D. Thrall, S. D. Colson, and H. P. Lu (2003). *Biophys. J.* **85**, 1826–1838.
24. G. S. Harms, G. Orr, and H. P. Lu (2004). *Appl. Phys. Lett.* **84**, 1792–1794.
25. T. Ha, A. Y. Ting, J. Liang, W. B. Caldwell, A. A. Deniz, D. S. Chemla, P. G. Schultz, and S. Weiss (1999). *PNAS USA* **96**, 893–898.
26. T. Ha, X. Zhuang, H. D. Kim, J. W. Orr, J. R. Williamson, and S. Chu (1999). *PNAS USA* **96**, 9077–9082.
27. S. Brasselet, E. J. G. Peterman, A. Miyawaki, and W. E. Moerner (2000). *J. Phys. Chem. B* **104**, 3676–3682.
28. G. S. Harms, L. Cognet, P. H. Lommerse, G. A. Blab, and T. Schmidt (2001). *Biophys. J.* **80**, 2396–2408.
29. H. Murakoshi, R. Iino, T. Kobayashi, T. Fujiwara, C. Ohshima, A. Yoshimura, and A. Kusumi (2004). *Proc. Natl. Acad. Sci. USA.* **101,** 7317–7322.
30. G. S. Harms, L. Cognet, P. H. Lommerse, G. A. Blab, and T. Schmidt (2001). *Biophys. J.* **80**, 2396–2408.
31. A. Kusumi, and Y. Sako (1996). *Curr. Opin. Cell. Bio.* **8**, 566–574.
32. O. H. Willemsen, M. M. Snel, A. Cambi, J. Greve, B. G. De Grooth, and C. G. Figdor (2000). *Biophys. J.* **79**, 3267–3281.
33. G. S. Harms, L. Cognet, P. H. Lommerse, G. A. Blab, and T. Schmidt (2001). *Biophys. J.* **80**, 2396–2408.
34. G. S. Harms, G. Orr, M. Montal, B. D. Thrall, S. D. Colson, and H. P. Lu (2003). *Biophys. J.* **85**, 1826–1838.
35. Th. Schmidt, G. J. Schuetz, H. J. Gruber, and H. Schindler (1996). *Anal. Chem.* **68**, 4397–4401.
36. G. S. Harms, L. Cognet, P. H. Lommerse, G. A. Blab, H. Kahr, R. Gamsjager, H. P. Spaink, N. M. Soldatov, C. Romanin, and T. Schmidt (2001). *Biophys. J.* **81**, 2639–2646.
37. G. S. Harms, G. Orr, M. Montal, B. D. Thrall, S. D. Colson, and H. P. Lu (2003). *Biophys. J.* **85**, 1826–1838.
38. G. S. Harms, L. Cognet, P. H. Lommerse, G. A. Blab, and T. Schmidt (2001). *Biophys. J.* **80**, 2396–2408.
39. G. S. Harms, L. Cognet, P. H. Lommerse, G. A. Blab, and T. Schmidt (2001). *Biophys. J.* **80**, 2396–2408.
40. G. S. Harms, L. Cognet, P. H. Lommerse, G. A. Blab, H. Kahr, R. Gamsjager, H. P. Spaink, N. M. Soldatov, C. Romanin, and T. Schmidt (2001). *Biophys. J.* **81**, 2639–2646.
41. G. S. Harms, L. Cognet, P. H. Lommerse, G. A. Blab, and T. Schmidt (2001). *Biophys. J.* **80**, 2396–2408.
42. G. S. Harms, L. Cognet, P. H. Lommerse, G. A. Blab, and T. Schmidt (2001). *Biophys. J.* **80**, 2396–2408.
43. G. S. Harms, L. Cognet, P. H. Lommerse, G. A. Blab, and T. Schmidt (2001). *Biophys. J.* **80**, 2396–2408.
44. Th. Schmidt, G. J. Schuetz, H. J. Gruber, and H. Schindler (1996). *Anal. Chem.* **68**, 4397–4401.
45. G. S. Harms, L. Cognet, P. H. Lommerse, G. A. Blab, and T. Schmidt (2001). *Biophys. J.* **80**, 2396–2408.
46. A. Schenk, S. Ivanchenko, C. Rocker, J. Wiedenmann, and G. U. Nienhaus (2004). *Biophys. J.* **86**, 384–394.
47. T. Nagai, K. Ibata, E. S. Park, M. Kubota, K. Mikoshiba, and A. Miyawaki (2002). *Nat. Biotechnol.* **20**, 87–90.
48. R. E. Campbell, O. Tour, A. E. Palmer, P. A. Steinbach, G. S. Baird, D. A. Zacharias, and R. Y. Tsien (2002). *Proc. Natl. Acad. Sci. USA* **99**, 7877–7882.
49. T. Nagai, K. Ibata, E. S. Park, M. Kubota, K. Mikoshiba, and A. Miyawaki (2002). *Nat. Biotechnol.* **20**, 87–90.
50. G. S. Harms, L. Cognet, P. H. Lommerse, G. A. Blab, and T. Schmidt (2001). *Biophys. J.* **80**, 2396–2408.